Proceedings of the 20th International Conference on Soil Mechanics and Geotechnical Engineering– Rahman and Jaksa (Eds)

Hydromechanical analysis of structure-soil-interactions at the flood barrier "Eidersperrwerk" in Germany

Analyse hydromécanique des interactions structure-sol du barrage de protection du littoral "Eidersperrwerk" en Allemagne

Denis Maier, Héctor Montenegro & Bernhard Odenwald
Geotechnical Department, Federal Waterways Engineering and Research Institute, Karlsruhe, Germany, hector.montenegro@baw.de

Thomas Nuber
Geotechnical Engineering in Coastal Areas, Federal Waterways Engineering and Research Institute, Hamburg, Germany

ABSTRACT: During maintenance works in the "Eidersperrwerk", one of the largest flood barrier structures in Germany, a monitoring system was established to observe the groundwater heads underneath as well as the deflection of the structure. Furthermore, a pressure relief system was installed to control the groundwater heads if necessary. The observed response of groundwater head to several measures during the maintenance works revealed rather complex soil–structure interactions. Emptying of the chambers as well as operation of the pressure relief system affected the groundwater heads underneath the structure in a predominantly nonlinear fashion. A numerical study based on a coupled hydromechanical model (poroMechanicalFoam) was able to reproduce accurately the observed groundwater head responses underneath the structure and yielded valuable insights into the role of gas entrapment in the seabed on soil-structure-interactions under mechanic and/or hydraulic loading.

RÉSUMÉ : Durant l'aménagement du barrage de l'Eider, l'une des plus grandes structures de protection du littoral en Allemagne, un système de suivi du site a été installé comprenant la charge hydraulique en dessous de la structure et les déformations de l'ouvrage. En outre, un système de relaxation hydraulique a été établi afin de pouvoir régler la charge hydraulique maximale sous la structure. L'observation de l'évolution de la charge hydraulique suite à différentes mesures de maintenance indique des interactions sol-structure complexes. La vidange des réservoirs et la mise en marche du système de relaxation hydraulique influent principalement de manière nonlinéaire sur la charge hydraulique en dessous de l'ouvrage. Une étude numérique basée sur une modélisation hydro-mécanique couplée (poroMechanical-Foam) reproduit avec précision le développement des charges hydrauliques en dessous de l'ouvrage. Ainsi, l'étude fournit un aperçu de l'impact de gaz occlus dans le fond marin sur les interactions sol-structure sous charge mécanique et/ou hydraulique.

KEYWORDS: soil–structure interactions, coupled flow-deformation model, geotechnical engineering, coastal.

1 INTRODUCTION

The "Eidersperrwerk" is located at the Westcoast of the German state Schleswig-Holstein in the estuary of the river Eider. With a length of approx. 188 km the Eider drains an area covering almost the entire northwestern part of Schleswig-Holstein. In the year 1967 - after one of the most severe storm surges of the younger history - a coastal protection scheme was adopted by the construction of flood barrier the so-called "Eidersperrwerk". The total length of the "Eidersperrwerk" is 240 m and it consists out of five chambers.

Between 2014 and 2018 extensive overhaul measures of the "Eidersperrwerk" were necessary requiring each chamber being emptied completely for several months. According to structural analyses the stability against uplift of the chamber was assured for ground water heads below NHN + 1.30 m. Risk considerations led to the installation of a ground water monitoring-system underneath the base of the chambers and of a pressure relief system for counteractions if necessary.

2 CONSTRUCTION AND FOUNDATION OF THE "EIDERSPERRWERK"

The "Eidersperrwerk" consists of with five separate chambers. Each chamber ranging over a length of 40 m and a width of 35 m (figure 1). Each chamber is bordered by concrete carriers. A massive concrete beam crosses the entire construction. Steel gates between the concrete carriers at both sides of each chamber permit an independent closing of each chamber providing thus a double dike-safety.

Figure 1. Aerial view of the flood barrier "Eidersperrwerk" (https://izw-medienarchiv.baw.de)

The floor of each chamber consists of a reinforced concrete slab of a thickness of 0.8 m founded on 42 piles which were driven into a deep lying bearing layer. The subsoil underneath the concrete slabs consists of sand and clay layers of approx. 5 m each. The concrete slabs are entirely surrounded by sheet pile walls which are embedded into the clay soil layer, so that the subsurface beneath the slabs is vertically and horizontally hydraulically confined (figure 2).

3 MONITORING SYSTEM

After emptying the chambers the stability of the concrete slab against uplift is only warranted up to a ground water head of NHN + 1.30 m. In spite of the hydraulic confinement through the sheet pile walls and the low permeability clay layer barriers ground water observations indicated a hydraulic connection

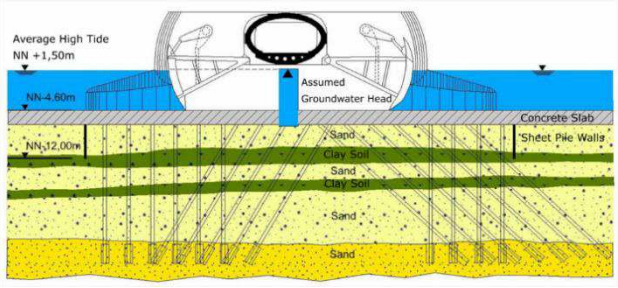

Figure 2. Cross-section of the "Eidersperrwerk"

between the sand aquifer and the tidal influenced North-Sea. In spite of the hydraulic confinement of the subsurface underneath the chambers it was presumed that under certain hydrological conditions ground water heads could be exceeded the critical value (Cordes, 1971).

These considerations required an observation system during the overhaul measures as well as a pressure relief system for counteractions. Thus, pressure transducers were installed in all four corners of each chamber to monitor the ground water heads (figure 3). In addition, two extensometers were installed in the middle of the chamber to observe any movements of the slab in response to head variations beneath the structure. Here, two telescopic rods with a length of approx. 5 m fixed between the concrete beam and the concrete slab were installed. The telescopic rods were equipped with temperature sensors for the compensation of temperature variations on the measurements.

The monitoring included the water levels in the chambers as well as of the river Eider and the North-Sea, which permitted to relate the observed heads below the structure to the external hydraulic conditions. Furthermore, a climate station was set up. With permanent pressure and deformation observation systems and the recording of external water levels a redundant monitoring of the structural response to any overhaul measures and the corresponding hydrological loadings was achieved

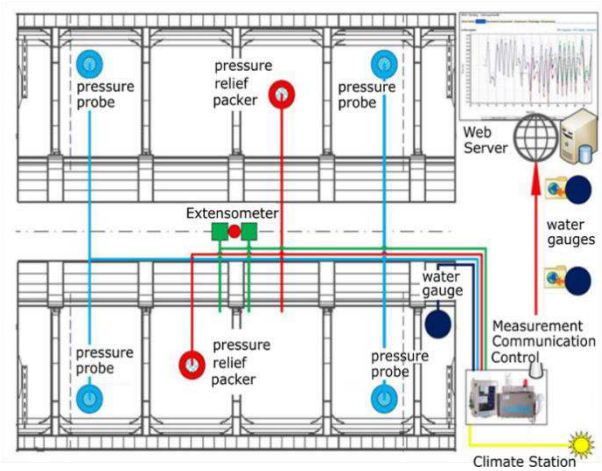

Figure 3. Set-up of the monitoring system (top-view)

In order to prevent any flooding of the chambers during the maintenance works, a pressure relief system was designed as passive ground water extraction wells. Due to the confined ground water conditions just a small volume of extracted ground water would provide a sufficient relief. These assumptions were verified by preliminary hydraulic tests.

4 PORE PRESSURE RESPONSE TO TIDAL DYNAMICS

The hydrographs of the installed pressure transducers probes displayed a damped response to the tidal fluctuations as shown exemplary for chamber 1 in fig. 5. A detailed analysis reveals that the head reacts without any delay to tidal fluctuations, which indicates that groundwater head responses primarily to mechanical load from fluctuating total stress on the chamber floor. A hydraulic response would involve pore pressure propagation and groundwater fluxes and thus require a certain time to reach the peaks.

The influence the emptying of the chamber, on the groundwater head below the concrete structure is evident in the drop of groundwater head. The removal of the water load upon emptying the chamber represents a static load change (variation of total stress) in the sandy subsoil. Remarkable, during and after the emptying of the chambers the ratio between the mean amplitudes of the tidal loading and the ground water heads (damping factors) reduces considerably.

Although, it was not necessary to relief the pressure a test of the pressure relief system was considered. The groundwater responded to the pressure relief, a hydraulic load change, comparable to the reduction in total stress from emptying the chamber. The groundwater head dropped and the amplitude reduced further. In the course of time the groundwater head ascended to its mean original value while the amplitudes grew as well however without reaching the values observed upon emptying the chamber. A second test operation of the relief system produced exactly the same effect on mean and amplitude of the groundwater head.

The gradual rise of the groundwater head permitted the assessment of the hydraulic conductivity of the confining clay-layer assuming the sheet-pile wall to be impermeable. The head rise following the test-runs of the relief system took several weeks which confirmed the assumption of a hydraulic confinement of the subsurface below the chambers due to the sheet-pile walls and a clay layer of low hydraulic conductivity.

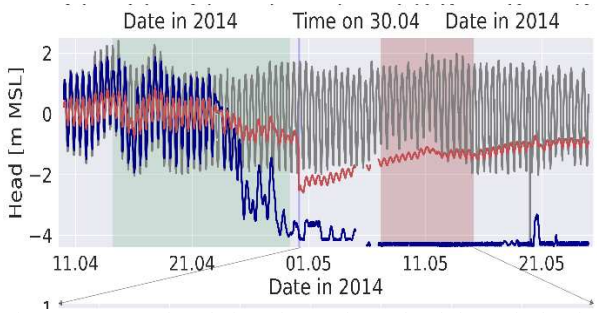

Figure 4. Temporal evolution of groundwater heads beneath chamber 1 (red), chamber water level (blue) and tidal fluctuations outside the chamber (grey). Green, blue and red zones mark the date ranges for the numerical investigations presented below

During the overhaul of the first four chambers the observed ground water heads never exceed values higher than NHN +1.3 m. Thus, the safety against an uplift of the concrete slab was given at all times during the overhaul of those chambers. Here, counteractions were not necessary. Though, during the overhaul of chamber 4 the observed groundwater heads indicated a hydraulic link between the chamber and the subsurface presumably due to a fracture in the concrete slab. To confirm this assumption colored water was infiltrated into the sandy subsurface layer through the pressure relief well applying overpressure. Here, the colored water flew out at two spots of a joint of the concrete slab so that the leak could be localized and fixed.

During the maintenance works in chamber 5 the ground water heads showed almost no damping in respect to the tidal loading which indicated that the hydraulic confinement of the sandy layer below the structure was not effective. Here, either leakage through defect sheet pile wall locks or a high hydraulic conductivity respectively a small thickness of the underlying clay layer was assumed. Due to the hydraulic connection high groundwater heads were to be anticipated during high water events. Here indeed the groundwater relief system hat to be applied for 16 times during the overhaul works. Without these

relief measures the groundwater heads would have reached the critical value requiring a rapid flooding of the chamber.

5 OCEAN-STRUCTURE-SOIL-INTERACTIONS

A profound understanding of soil–structure interactions under tidal loading is essential for the design of any coastal structure and for the assessment the safety under maintenance works. These processes are rather complex due to the coupled behavior of the soil and the structure under periodic fluctuating water levels. Loading due to the wave and tidal dynamics may appear as variations of total stress above the impermeable structure (static loading) or pore pressure (hydraulic loading) above the permeable sea bed. Understanding of the observed groundwater head responses underneath the structure to maintenance works, total stress changes following the drying of the chambers and changes of the mean pore pressure level upon relief measures demanded a careful analysis along the principles of Biot's theory of poroelasticity. Within this context the responses of soil deformations and interstitial flows to external static and/or mechanic load variations depend predominantly on the elastic properties of the soil matrix (stiffness) and of the interstitial fluid. If the pores were completely filled with water, the assumption of an incompressible fluid would be reasonable. In the progression of the analysis it was realized that fluid compressibility enhanced by entrapped gas bubbles played a key role. The response of pore pressure to total stress changes is quite sensitive to the compressibilities of the matrix and the fluid. Even a small amount of entrapped gas most probably from biogenic origin may increase the compressibility of the water -gas mixture considerably [Motenegro & Köhler $]. Such an enhanced fluid compressibility resulted in reduced pore pressure responses to total stress variations. Astoundingly, variation of the pore pressure responses to total stress variations indicated that fluid compressibility varied with either mechanically (total stress variations upon emptying the chambers) or hydraulically (relief wells operations) induced mean pore pressure level changes. In order to reflect these effects a hydromechanical model was set up, which was able to consider gas entrapment and its effect on the compressibility of the interstitial fluid.

6 MODEL FORMULATION

We consider the structure and the soil to consist of a porous, linear elastic deformable solid material. The voids of the concrete structure is assumed to be filled with a single, incompressible fluid, while gas entrapment in the voids of the soil (degree of saturation below unity) is considered. Due to the slowness of the water level changes we assume quasi-static behavior and ignore non-isothermal effects. By reason of soil water storage the problem of coupled interstitial flow and deformation is intrinsically time-dependent. The unknown fields are the displacement **u** [L] of the solid and the pore-fluid (water-gas-mixture) pressure p [F/L^2].

6.1 *Governing equations*

The initial–boundary-value problem for coupled flow deformation can be written as:

$$\nabla \cdot \boldsymbol{\sigma} + \rho \boldsymbol{g} = (\boldsymbol{\sigma}' - \alpha\, p \boldsymbol{I}) + \rho \boldsymbol{g} = 0 \tag{1}$$

$$\alpha\, S \frac{\partial \varepsilon}{\partial t} + n \frac{dS}{dp}\frac{dp}{dt} + n \frac{S}{K_w}\frac{\partial p}{\partial t} + (1-n)\frac{S}{K_s}\frac{\partial p}{\partial t} = -\boldsymbol{\nabla} \cdot \boldsymbol{q_w} \tag{2}$$

These two equations represent the balance of linear momentum and balance of mass for the mixture, respectively. Note that the formulation uses the standard mechanics notation where stress is positive in tension and pressure is positive in compression. Here, is σ and σ' [F/L^2] the total and effective stress respective, p [F/L^2] the pore-fluid pressure, ρ [M/L^3] is the mixture density, **g** [L/T^2] is the gravity vector, n [-] is the initial porosity. Since the porous matrix is deformable variations in porosity are considered through the deformation rate term ∂ε/∂t [1/T]. For simplicity we do not consider these small variations and n in the storage terms in (2) is not updated. K_w [F/L^2] is the water bulk modulus and $\mathbf{q} = \theta\ \mathbf{v}$[L/T] is the seepage (Darcy) velocity relative to the velocity of solid displacement and **I** is the unit second-order tensor. The solid grains are considered as incompressible in the stress-strain range encountered in geotechnical engineering practice, therefore the Biot-Willis coefficient $\alpha = 1 - K/K_s$ [-] which relates the bulk modulus contrast between the matrix K [F/L^2] and the solid grains K_s [F/L^2] equals unity and the term considering K_s in (2) vanishes. In view of the immense bulk modulus of the water K_w (i. e. negligible water compressibility) compared to the bulk moduli of soils the term containing K_w in (2) ignored as well. The mixture density ρ [M/L^3] is related to the solid ρ_s [M/L^3] and fluid ρ_f [M/L^3] constituent densities as:

$$\rho = n\, \rho_f + (1-n)\, \rho_s \tag{3}$$

6.2 *Initial conditions*

Initial conditions for the unknown variables are prescribed as:

$$\boldsymbol{u}(\boldsymbol{x}, 0) = \overline{\boldsymbol{u}}_0(\boldsymbol{x}) \tag{4}$$

$$p(\boldsymbol{x}, 0) = \bar{p}_0(\boldsymbol{x}) \tag{5}$$

Where **x** [L] is the position vector within the domain.

6.3 *Boundary conditions*

The domain boundary is partitioned into surfaces Γ over which essential boundary conditions are applied:

$$\begin{aligned} &\boldsymbol{u}(\boldsymbol{x}, t) = \overline{\boldsymbol{u}}(\boldsymbol{x}, t) \ \text{ on } \Gamma_u \\ &\boldsymbol{\sigma}(\boldsymbol{x}, t) \cdot \boldsymbol{n}(x) = \bar{\boldsymbol{t}}(\boldsymbol{x}, t) \ \text{ on } \Gamma_t \\ &p(\boldsymbol{x}, t) = \bar{p}(\boldsymbol{x}, t) \ \text{ on } \Gamma_p \\ &\boldsymbol{q}(\boldsymbol{x}, t) \cdot \boldsymbol{n}(x) = \overline{\boldsymbol{q}}(\boldsymbol{x}, t) \ \text{ on } \Gamma_q \end{aligned} \tag{6}$$

where $\bar{u}$ is a prescribed displacement, $\bar{t}$ is a prescribed total traction, $\bar{p}$ is a prescribed pressure and $\bar{q}$ is a prescribed normal flux with **n** representing the normal vector. The combination of the boundary conditions depends on the application of displacements and/or stresses and the ability to release fluid at the respective boundary.

6.4 *Constitutive Relations*

The governing equation system is closed with several constitutive relationships. The tensor of effective stresses is related to the strain tensor **ε** [-] as

$$\boldsymbol{\sigma}' = \boldsymbol{C} : \boldsymbol{\varepsilon} \tag{7}$$

where **C** [F/L^2] is a fourth-order tensor of tangent moduli. Here an isotropic linear elastic stress–strain relationship between strain tensor and displacement field is considered. We adopt small-strain assumptions for simplicity (Cauchy's strain tensor).

$$\boldsymbol{\varepsilon} = \nabla \boldsymbol{u} = \frac{1}{2}(\nabla \boldsymbol{u} + \nabla^T \boldsymbol{u}) \tag{8}$$

Pore-fluid pressure gradient and seepage velocity are related by Darcy's law,

$$\boldsymbol{q} = -\boldsymbol{k} \cdot (\nabla p - \rho_f \boldsymbol{g}) \tag{9}$$

where **k** [L/T] is the tensor of the hydraulic conductivity and **g**

the vector of gravity. For simplicity no changes on the hydraulic conductivity with variations in saturation are considered.

Assuming the presence of entrapped gas bubbles within the pore space below the phreatic surface and ignoring surface tension effects at the gas-liquid interfaces virtually the same pressure in the liquid and gaseous phase can be expected. We adopt a Boyle-type variation of gas volume V_g [L^3] with pore pressure:

$$\frac{V_g}{V_{g0}} = \frac{S_g}{S_{g0}} = \frac{1-S}{1-S_0} = \frac{p_a}{p_a+p} \qquad (10)$$

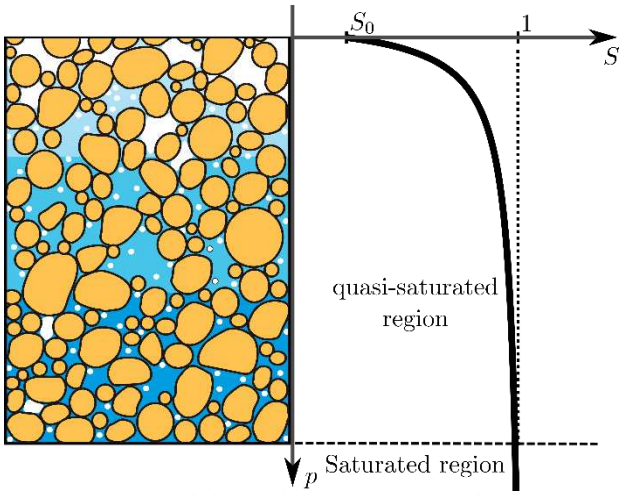

Figure 4. Adopted relationship between saturation and pore pressure in the quasi saturated zone due to gas entrapment.

This gas entrapment model requires only one parameter, the water saturation S_0 [-] corresponding to reference conditions at atmospheric pressure pa [F/L^2]. The value of S_0 depends on soil type and on the wetting circumstances. In soils with fluctuating ground water table values of $0.8 < S0 < 0.9$ have been reported. At the sea bed gas occlusions may largely result from biogenic processes. The compressibility of the entrapped gaseous phase enhances the ability to store and release water and accordingly a fluid pressure dependent storage C(p) [L^2/F] is defined:

$$C(p) = n\frac{dS}{dp} = n\,(1-S_0)\,\frac{p_a}{(p_a+p)^2} \qquad (11)$$

6.5 *Numerical model, model geometry and material properties*

To integrate the above derived coupled equations describing hydromechanical behaviour in porous media the finite-volume platform openFoam was used. Firstly designed for fluid dynamical analyses, the platform was extended to solid mechanics mainly by Jasak and Cardiff $. Tang et al. $ were among the first to extend the code for hydromechanical analysis in porous media. For the investigation hereafter, their code was extended to consider partial saturation and pore-pressure dependent storage as described in the previous chapter.

Though the hydromechanical model implementation was accomplished in full 3D the present analysis consists of a 2D plane strain model with linear elastic soil behavior for simplicity. Several material whose mechanical and hydraulic properties were estimated in preliminary studies are listed in Table 1. Figure 5 shows the structure and hydrogeological arrangement in the domain as well as the applied boundary conditions.

The sheet pile walls and concrete slap (black structures in Figure 5) were considered to be rather flexible for simplicity. Preliminary studies revealed that the stiffnesses of the structural components did not affect markedly the pore pressure responses, though convergence was severely affected with high-stiffness structural properties. It is to be stated that displacements depend on the selected stiffness of the soil and the structural materials, however, displacements were not in the scope of the present analysis.

Table 1. Material parameters used in the calculation.

Material	*sand*	*clay soil*	*sheet piles & concrete*
Young Modulus E (MPa)	45.0	45.0	45.0
Poisson ratio ν (-)	0.33	0.33	0.33
Ref. Saturation S_0 (-)	0.95	0.95	-
Hyd. conductivity k (m/s)	$1{\cdot}10^{-4}$	$3{\cdot}10^{-9}$	$1{\cdot}10^{-19}$
Porosity n (-)	0.25	0.25	-

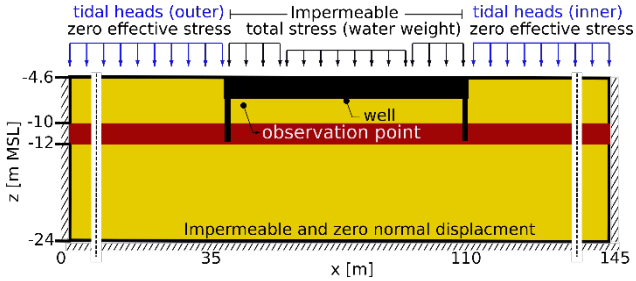

Figure 5. Geometry and boundary-conditions of the considered domain. Yellow regions correspond to sand, red regions to the clay layer and the sheet piles and concrete slab are in black.

Tidal heads for outer-Eider (coastal) and inner-Eider (inland) have been directly prescribed at the corresponding sea bed boundaries. Due to data losses in the recording of inner-Eider water levels during emptying of the chamber, the outer-Eider fluctuations were assigned on the inner-Eider boundary for that corresponding time period. The concrete slab boundary was assigned as impermeable and hence water level fluctuations were considered as total stress variations.

7 COMPARISON OF OBSERVED AND COMPUTED HEADS BELOW THE CONCRETE STRUCTURE

The observation point in Figure 5 was set in accordance with the position of the pressure probes in a depth of around 1.6 m underneath the top edge of the concrete slab.

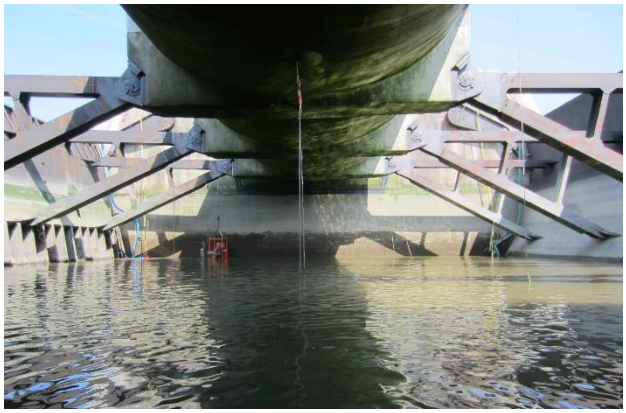

Figure 6. View of the closed chamber during emptying

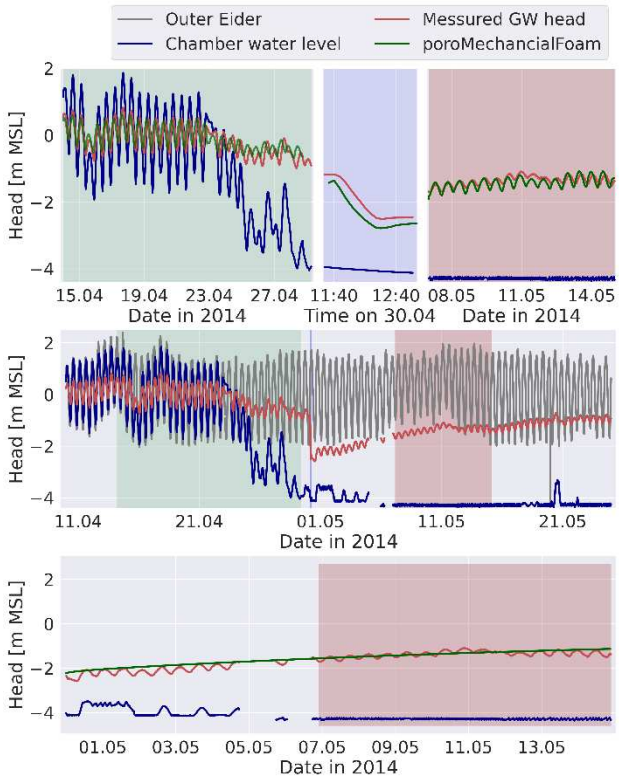

Figure 7. **Top**: Observed (redline) and calculated (green line) pressure heads during the considered phases, emptying of the chamber (green box), groundwater relief (blue box) and equilibration phase (red box). **Bottom**: Equilibration phase analyzed with a decoupled model (groundwater flow).

Figure 7 displays the observed and calculated pore pressure heads during different phases. The synchronous water level fluctuations of the pore pressure response underneath the concrete slab with the tidal fluctuations (Fig. 7. Top, green box) revealed that the former was triggered solely by mechanical loading variations. If groundwater flow was the driving force for the subsurface fluctuations, as previously assumed, a delayed pore pressure response would have been observed. These findings suggested hydraulically encapsulated conditions below the concrete slab due to the sheet pile walls and the underlying clay layer.

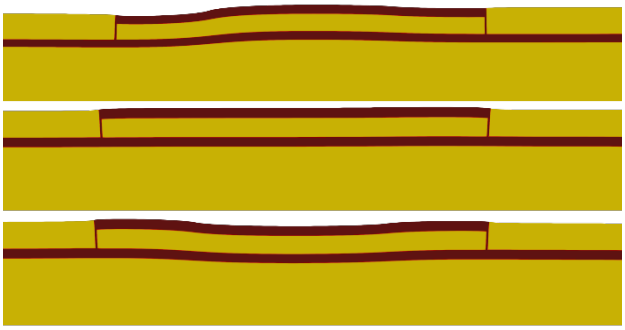

Figure 8. Computed elastic deformations (exaggerated) around the concrete structure with gates closed in response to tidal loading. **Top**: high water. **Middle**: mean water. **Bottom**: low water.

Under such "undrained conditions" the observed ratio between the amplitudes of the pore pressure underneath the concrete slab to variations of total stress (tidal water level fluctuations on the concrete slab) unambiguously indicated the presence of a compressible pore fluid which can be only explained by gas entrapment in the voids of the soil. The ratio of amplitudes of pressure head below the structure to tidal head fluctuations of around 0.3 proved to be quite sensitive to the assumed entrapped gas content hence S_0 was calibrated to the value of 0.95.

While the ratio of head amplitudes remains initially at around 0.3, after lowering the chamber water table the amplitude-ratio decreases to roughly 0.1. This decline reflects the reduction of the effective loading area. After lowering the water level in the closed chamber (see Fig. 8) the total stress variations occur only on the parts of the slab outside the gates of the chamber, which represent about one half of the total slab area (see Fig. 2).

Theoretically a reduction of the amplitude ratio was expected due to the decrease of total stress and accordingly pore pressure underneath the concrete slab following emptying. The pore pressure drop corresponds in the proposed Boyle-type storage model to an increase gas volume and hence in fluid compressibility. Consequently more subtle pore pressure response to total stress variations occur. However the pressure head drop of around 2.5 m upon emptying the chamber in the piezometric level of around 4 m below mSWL does not enhance the fluid compressibility as markedly as the reduction of the effective area prone to tidal loading after closing the gates.

Figure 8 displays largely amplified displacements and illustrates the hydromechanical responses to the tidal loading when the gates are closed and the chamber is empty. The major displacements occur on the concrete slab outside the gates, where the tidal fluctuations act as total stress variations. Figure 8; top shows the phase shift between the outer and inner tidal fluctuations. At this point in time the water level of the outer Eider has reached its maximum, while the inner Eider level is still rising. During the mean (Figure 8; middle) water level stage almost no displacements are visible. Finally upward displacements at the ends of the slab occur in response to low water levels (Figure 8; bottom).

Subsurface pressure head fluctuations during the emptying of the chamber remain intimately correlated with water level variations within the chamber as displayed in Fig. 7, top, green field. The calculated pressure heads agree staggeringly well in the timespan before the emptying of the chamber. During the emptying computed pressure heads do not follow strictly the oscillations in chamber water level anymore. This, however, is the result of the aforementioned need to prescribe the coastal water level fluctuations on the inland boundary due to outages of measurements during that particular period of time. The water levels on the coastal side of the structure are somewhat phase-shifted in respect to the inner Eider water levels as mentioned above.

In order to validate the assumptions of hydraulic encapsulation below the structure the period following the pressure relief (red colored period in Fig. 7) was examined. Again a quite decent agreement between observation an calculation was achieved. After applying the correct water levels of the inner Eider the phase shift disappeared.

Coupled simulation requires computation time due the necessity to evaluate flow and deformation iteratively. In order analyze the whole equilibration period the hydromechanical coupling was disabled performing accordingly a mere groundwater flow (rigid porous media) analysis. Inner and outer tidal heads were kept constant at the mean value (0 m MSL) for simplicity. Equilibration results from groundwater flow through the clay layer in response to the head differences induced by the pressure release operations underneath the slab. The observed an computed response of pressure head underneath the concrete structure are displayed Fig. 7, bottom. Due to the constant head boundary conditions the calculated heads do not exhibit oscillatory behavior. However, the long-term equilibration following groundwater flow from below the clay layer is captured, again with surprising precision, by the uncoupled model as well. This analysis confirmed a rather impermeable encapsulation of the soil underneath the concrete slab. In the time scale of tidal loading undrained conditions can be assumed and consequently the pore pressure variations are not affected by

tidally induced groundwater flow.

8 SUMMARY AND CONCLUTION

The installed monitoring and pressure relief system proved to be robust and allowed uninterrupted maintenance works under the exceptional conditions of emptied chambers. The data collected during the maintenance works revealed complex interactions between tidal loading and pore pressure underneath the concrete structure. These interactions were analyzed based on a rather simple vertical plane hydromechanical model. It was possible to identify a rather encapsulated domain underneath the concrete structure bounded by sheet pile walls and a clay-layer. Under such “undrained conditions” the observed pore pressure response was merely induced by mechanical loading following tidal water level changes on the concrete slab. The ratio in amplitudes of the tidal loading and the pore pressure response disclosed the influence of gas entrapment in the voids of the subsurface soil and hence the compressibility of the por fluid (gas-water mixture). The gas Saturation was identified to be 5 % and it can be presumed that such an amount of gas in the sea bed must have a biogenic origin.

The numerical study based on a rather simple vertical plane model (Finite Volume Method), poroMechanicalFoam, considering hydromechanical coupling was able to reproduce accurately the observed groundwater head responses underneath the structure and yielded valuable insights into the role of gas entrapment in the seabed on soil-structure-interactions under mechanic and/or hydraulic loading.

9 ACKNOWLEDGEMENTS

@Thomas: Thanks to WSV-Tönning and to Gerd Siebenborn.

10 REFERENCES

Cordes, F., 2015. Eiderdamm Hundeknöll-Vollerwiek: II. Teil Bau des Eidersperrwerks, Die Bautechnik (48) Vol. 10 (1971).

De Wiest, R.J.M, 1966. On the storage coefficient and the equations of North flow. Journal of Geophysics Research, Vol. 71, S. 1117-1122.

Ewers J. (2016): Porenströmung als Auslöser für Erosion? Tagungsband zum "Johann-Ohde-Kolloquium". BAW und TU Dresden. BAW-Mitteilungen Nr. 99.

Fredlund D. G., Rahardjo H., Fredlund M. D. (2012): Unsaturated Soil Mechanics in Engineering Practice. John Wiley & Sons.

Köhler, H.-J.; Montenegro, H. (2003): Investigations regarding soils below phreatic surface as unsaturated porous media. In: Unsaturated Soils: Numerical and Theoretical Approaches: Proceedings of the International Conference "From Experimental Evidence Towards Numerical Modeling of Unsaturated Soils", Weimar, Germany, September 18-19.

Montenegro, H., Stelzer, O. (2014). Untersuchung des Einflusses von Gaseinschlüssen unterhalb des Grundwasserspiegels auf Druckausbreitung und Bodenverformungen mittels gekoppelter FE-Berechnungen. Ohde Kolloquium 2014 Mitteilungsheft 19. Institut für Geotechnik. Technische Universität Dresden.

Montenegro, H., Stelzer, O. Odenwald, B. (2015): Parameterstudie zum Einfluss von Gasbläschen im Grundwasser auf Porenwasserdruck und effektive Spannung bei Auflast- oder Wasserspiegeländerungen. BAW Mitteilungen Nr. 98.

Montenegro, H.; Köhler, H..-J. and Holfelder, T. (2003): Inspection of excess pressure propagation in the zone of gas entrapment below the capillary fringe. Proceedings, International Conference "From Experimental Evidence towards Numerical Modelling of Unsaturated Soils", Weimar, Germany, Vol. 2, September 2003.

Paton, J. and Semple (1961), N.G. Investigation of the Stability of an Earth Dam Subject to Rapid Drawdown including Details on Pore Pressures recorded during a Controlled Drawdown Test., in Pore Pressure and Suction in Soils, pp. 85-90, Butterworth, London.

Pinyol, N. M.; Alonso, E. E and Olivella, S. (2008): Rapid drawdown in slopes and embankments. Water Resources Research 44, 2008 W00D03.

Stelzer, O. (2016): Zur Berücksichtigung der Kopplung von Grundwasserströmung und Bodenverformung bei der numerischen Berechnung der Porenwasserdruckverteilung. BAW-Mitteilungen Nr. 99.

Stelzer, O., Montenegro, H., Odenwald, B. (2014) Consolidation Analyses Considering Gas Entrapment below the Phreatic Surface. Numerical Methods in Geotechnical Engineering. Proceedings. CRC Press.

Wang, H. F. (2000): Theory of Linear Poroelasticity with Applications to Geomechanics and Hydrogeology. Princeton University Press.